PHYSICAL REVIEW B VOLUME 27, NUMBER 2 15 JANUARY 1983

Time-resolved conductance and reflectance measurements of silicon during pulsed-laser annealing

G. J. Galvin, Michael O. Thompson, and J. W. Mayer
Department of Materials Science, Cornell University, Ithaca, New York 14853

P. S. Peercy
Sandia National Laboratories, Albuquerque, New Mexico 87185

R. B. Hammond and N. Paulter
Los Alamos National Laboratory, Los Alamos, New Mexico 87544
(Received 12 July 1982)

The dynamics of silicon solidification from the melt during pulsed-ruby-laser annealing have been investigated with the use of time-resolved electrical-conductance and optical-reflectance measurements. Melt duration was found to increase with laser-energy density to over 450 nsec at the highest energy used (3.1 J/cm^2). Resolidification velocity was found to vary with time and laser-energy density over a range of 2 to 3 m/sec. The melt threshold was observed to be 0.8 J/cm^2. Measurements of the laser energy absorbed in the sample were made to determine energy coupling parameters for use in numerical calculations. The numerical calculations, based on a thermal model for laser melting, are found to be in good agreement with the experimental results.

I. INTRODUCTION

In pulsed-laser annealing of semiconductors, the absorbed laser energy has been shown to melt a thin layer (<0.8 μm) of the near-surface region of the irradiated solid.[1–5] Melting is initiated at the surface and the melt front then propagates into the solid. The molten layer then resolidifies as the heat produced by the absorbed energy is conducted into the substrate. The velocity of the solidification front, as the liquid-solid interface moves back toward the surface, is of central importance from both theoretical and applied viewpoints. From a theoretical viewpoint, precise knowledge of this resolidification velocity is required for detailed examination of either thermal[6,7] or nonthermal[8,9] models of laser annealing and for investigations of solidification dynamics at very high resolidification rates (>1 m/sec). From an applied viewpoint, the resolidification velocity is the primary parameter in segregation, trapping, and phase separation of impurities in semiconductors[10,11] and in the defect structure of the annealed material.[12]

A variety of experiments have been performed to study the laser-annealing process. Such experiments can be divided into two categories:

(1) Experiments performed on samples during the annealing. Such experiments can yield information on the real-time behavior of the pulsed-laser-annealing process. For example, optical-reflectance or -transmission measurements can be used to determine the melt duration. However, such measurements are insensitive to the melt depth and the dynamics of the melting and resolidification processes.

(2) Post-annealing experiments, such as ion-channeling and electron microscopy. These experiments can give information on the melt depth but cannot yield direct information on the dynamics of the melting and resolidification processes. For these experiments such dynamics must be inferred from theoretical calculations.

We have recently shown[13,14] that direct experimental observations of annealing dynamics can be obtained by measurement of the electrical conductance of a Si sample during laser annealing. Si becomes metallic upon melting, resulting in greatly increased electrical conductance and optical reflectance over that of the solid phase. Consequently, the electrical conductance of the sample during irradiation provides a measure of the volume of molten material as a function of time. From this information, one can obtain the melt-front velocity, the maximum melt depth, the resolidification velocity, and the melt duration. Transient electrical-conductance measurements during pulsed-laser annealing were previously used to determine the melt depth and solidification-front velocity in Au-doped single-crystal Si (Ref. 13) and both the melt- and solidification-front velocity of silicon on sap-

 ©1983 The American Physical Society

phire.[14,15]

This paper reports the use of simultaneous optical-reflectance and electrical-conductance measurements to examine the dynamics of pulsed-laser annealing. In addition, energy-absorption measurements[16] are used to provide the energy coupling parameters, specific to an individual sample, to be used in computer calculations of the temperature profiles and melt depths. Simultaneous measurement of reflectance and conductance allows corroboration of melt duration between the two methods. Melt depths and solidification-front velocities are calculated from the conductance measurements and compared with numerical calculations based on a simple thermal-melting model.

II. EXPERIMENTAL DETAILS

Wafers of Si⟨111⟩ with 2000 Å of Au evaporated on them were sealed in a quartz tube and annealed for 15 min at 1250 °C. The wafers were then etched in aqua regia and repolished. This procedure introduced $\sim 10^{17}$ atoms Au cm^{-3} into the Si and reduced the carrier lifetime so that the photoconductive response would not mask the entire melt conductance.[17] Sample lengths of 5.8 mm were used. The sample widths were 0.25 mm, yielding a length-to-width (l/w) ratio of 23. Al was evaporated onto the Au-doped Si, and the Al was photolithographically etched to form contacts at either end of the bar.

Irradiation was provided by a Q-switched ruby laser [pulse length 30 nsec FWHM (full width at half maximum)]. A diagram of the experimental setup is shown in Fig. 1(a). The quartz-beam homogenizer[18] provides uniform ($\pm 5\%$) illumination over the entire sample including at least part of all contacts. Incident laser energy was varied by neutral density filters to ensure that the laser pulse shape was independent of energy. This method was used since the pulse shape can influence the melting behavior.[19] Energy calibration was obtained using a calorimeter, and the calibration was checked periodically during the experiments. Energy for each laser pulse was measured from a split-off portion of the beam monitored by a fast and an integrating photodiode. Another photodiode provided the trigger signal for all oscilloscopes used in the measurements to ensure consistent timing.

A bias voltage V_b, typically 40 V, was applied across the end contacts of the sample. Fast capacitors were mounted near the contacts to keep transients on the bias voltage to less than 3 V. The current through the sample was measured by the voltage across the 50-Ω (R_L) scope input. Figure 1(b) shows a schematic illustration of the experiment.

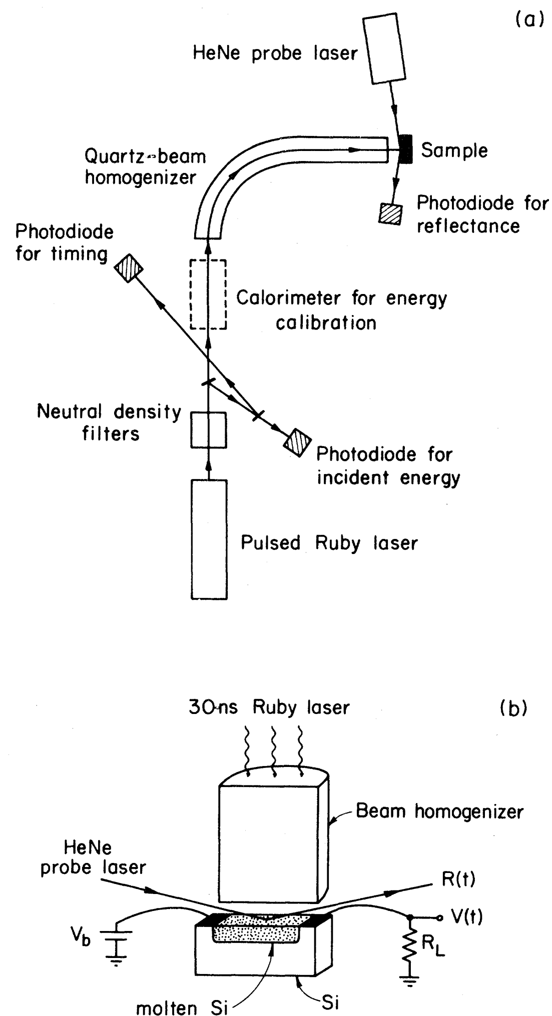

FIG. 1. (a) Experimental setup for simultaneous measurement of electrical conductance and optical reflectance. (b) Schematic diagram of the experiment.

Data in the form of the voltage across the load R_L were fed directly into a transient digital analyzer system consisting of Tektronics 7912ADs tied to a minicomputer and floppy disk storage. This data-acquisition system allowed analysis of the data immediately after each laser shot.

A HeNe laser was used to probe the surface reflectivity $R(t)$ during irradiation with the ruby laser. The HeNe laser beam was placed at a grazing angle to the sample surface because of the geometry restrictions imposed by the beam homogenizer. Because the reflectance measurements were made at grazing angles, no attempt was made to determine absolute reflectivities from the reflectance. Rather, the reflectance measurements were used to confirm that melting had occurred, to determine the time

during the laser pulse at which the melt started, and to measure the melt duration. The reflectance data was also fed directly into the transient digital analyzer system.

The fraction of the laser energy absorbed in both the liquid and solid phases was measured using a calorimetric technique.[16] Since different surface conditions can alter the reflectivity, and hence the absorbed energy, these measurements were made on the same samples as were used for the conductance measurements.

III. EXPERIMENTAL RESULTS

A. Electrical conductance

The time-dependent voltage $V(t)$ is measured across a 50-Ω scope load, using the experimental configuration shown in Fig. 1(a). Figure 2(b) shows $V(t)$ data for a variety of incident laser energy densities. These data were taken on a single-crystal Au-doped Si bar 5.8-mm long and 0.25-mm wide ($l/w=23$) with a 40-V bias voltage. This relatively high bias voltage was used to overcome any non-Ohmic features in the contact resistance. Similar measurements were made on samples having l/w ranging from 5.8 up to 50 with qualitatively similar results. A large l/w ratio results in the resistance of the sample, even at maximum melt depth, being much larger than the contact resistance. Consequently, uncertainty in the value of the contact resistance is at most a 2% error in the data (for a $l/w=23$). Four-point-probe measurements were also made to verify that the contact resistance was indeed on the order of 2—3 Ω.

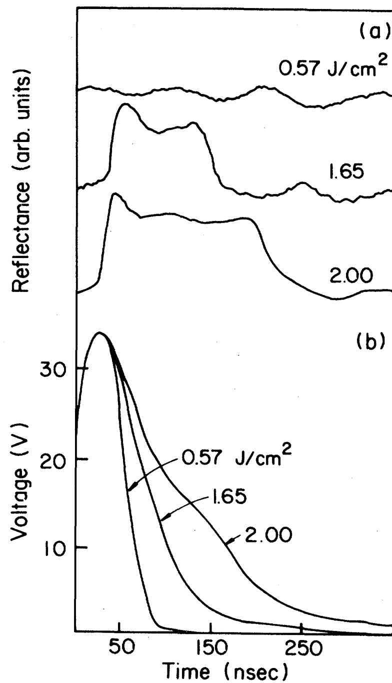

FIG. 2. (a) Signal from the reflected HeNe probe laser as a function of time for three incident laser energy densities. The 0.57-J/cm^2 case is below the melt threshold and the other two data, 1.65 and 2.00 J/cm^2, are above the melt threshold. (b) Electrical conductance, as measured by the voltage across the scope-load resistor, as a function of time obtained simultaneously with the reflectance data in (a).

The signal observed for energy densities below the melt-threshold energy density, $E_m \sim 0.8$ J/cm^2, is produced by photoconductivity in the Si. Although the photoconductive response is greatly reduced compared to that of Si without the Au doping, it still obscures the first 80 nsec of the molten-Si conductance. Lower lifetime material such as silicon on sapphire can be used to overcome this limitation.[14] Above 0.8 J/cm^2 the transient voltage curves show the conductance increasing in magnitude and duration after the photoresponse. The value of the conductance can be calculated from the voltage data as discussed in Sec. IV A.

B. Comparison of electrical and optical measurements

Changes in the optical reflectivity, which occur upon melting due to the metallic nature of molten Si, were correlated with the transient electrical conductance. This correlation was accomplished by simultaneous measurement of the optical reflectance, using a HeNe probe laser, and the electrical conductance. The results are shown in Fig. 2 for various incident laser energy densities. The reflectance measurements directly yield the time during the laser pulse at which melting occurred and the duration of the melt. Because of the large photoresponse which obscures the conductance signal from liquid Si for melt durations less than 80 nsec, reflectance measurements are more sensitive to the melt threshold than are the conductance measurements.

C. Energy absorption

Precise numerical calculations of the temperature profiles and melt dynamics require accurate values of the optical coupling to the sample in both the liquid and solid phases. Although reasonable agreement between theoretical calculations and experimental measurements was previously obtained[13] using energy absorption measured on different samples than those used for the transient conductance measurements, the optical coupling can vary from sam-

ple to sample depending on surface preparation and treatment.[20] We therefore measured the absorbed energy on the same sample as was used for the conductance measurements.

These energy-absorption measurements were made by attaching the sample to a thermocouple and measuring the temperature rise at the back surface of the sample as a function of incident laser energy.[16] This technique provides the melt-threshold energy and the fraction of the incident energy absorbed in both the solid and liquid phases. Figure 3 shows the temperature rise versus time for the Si sample prior to performing transient conductance measurements. The break in the curve at 0.82 J/cm^2 is the melt-threshold energy. From the slope of the curve prior to and after the threshold, the energy absorption in the solid and liquid phases, respectively, can be obtained by

$$A=\frac{\Delta T m C_p}{a}\ , \tag{1}$$

where m is the mass of the sample, a is the area of the sample, C_p is the heat capacity, and ΔT is the slope of the ΔT-vs-E curve.

IV. DISCUSSION

A. Melt depths

Analysis of the transient conductance data, Fig. 2, requires converting the observed voltage trace to a conductance, and then to a melt depth. The conductance $\sigma(t)$ in Ω^{-1}, is related to the voltage transient $V(t)$ by

$$\frac{1}{\sigma(t)}=R(t)=R_L\left[\frac{V_b}{V(t)}-1\right]-R_c\ , \tag{2}$$

where V_b is the bias voltage, R_L is the scope-load resistance (50 Ω), and R_c is the contact resistance. This observed conductance is composed of three parallel contributions: $\sigma_p(t)$ due to photoconduction, $\sigma_m(t)$ due to the molten-Si layer, and $\sigma_t(t)$ due to thermally generated carriers in the solid Si, as shown in the equivalent circuit in Fig. 4(a). Figure 4(b) shows the voltage transient $V(t)$ and observed conductance $\sigma(t)$ for an incident energy density of 1.96 J/cm^2. For energy densities below the melt threshold, the only contribution to the conductance is the photoconductance, the duration of which is indicated by the dashed line in Fig. 4(b). During the photoresponse the sample resistance is essentially zero, allowing the contact resistance to be calculated from the peak photoresponse voltage. This peak voltage saturates starting at energies well below the melt threshold, indicating that σ_p does indeed approach infinity. However, to accurately calculate the contact resistance, the transient drop in the bias voltage (measured to be 2—3 V) must also be included. These calculations result in a contact resistance of the order of 2—3 Ω. As mentioned in Sec. III A,

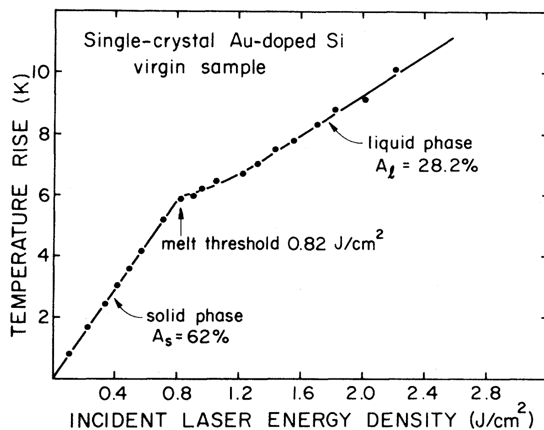

FIG. 3. Temperature rise at the back surface of the sample as a function of incident laser energy density for single-crystal Au-doped Si.

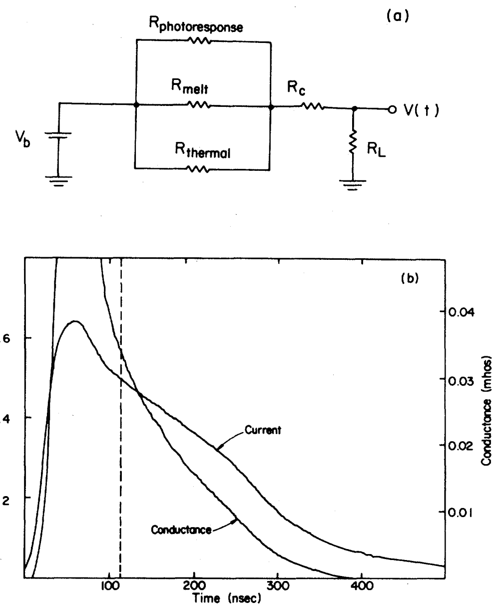

FIG. 4. (a) Equivalent circuit showing the three contributions to the observed conductance signal. (b) Current through the sample and conductance of the sample as a function of time for an incident laser energy density of 1.96 J/cm^2. Dashed line indicates the duration of the photoconductance.

this resistance is small compared to the sample resistance during melt, and hence it does not substantially affect the melt-depth calculations.

The time at which solidification is complete can be determined from the reflectance data. The conductance which still exists upon termination of the resolidification is σ_t, the conductance due to thermally generated carriers.

The equivalent circuit of Fig. 4(a) can be solved for the conductance due to the molten Si alone,

$$\sigma_m(t)=\sigma(t)-\sigma_p(t)-\sigma_t(t)\ , \tag{3}$$

where each conductance on the right-hand side is obtained from the appropriate voltage data using Eq. (2).

The melt depth $d(t)$ can be calculated directly from the conductance of the molten layer,

$$d(t)=\sigma_m(t)\rho l/w\ , \tag{4}$$

where ρ is the resistivity of molten Si ($80\,\mu\Omega\,\mathrm{cm}$),[21] and l/w is the length-to-width ratio of the molten region. A family of melt-depth—versus—time curves for various incident laser energy densities is shown in Fig. 5.

B. Numerical calculations

Detailed numerical calculations similar to those of Baeri *et al.*[22] and Wood and Giles[23] were performed to obtain melt depths and solidification-front velocities to compare with the experimental results. The calculations were performed using a central difference algorithm to compute the temperature profiles as a function of depth and time in the Si. A simple heat-flow model for the solification is used in which the latent heat of fusion liberated at the advancing liquid-solid interface is balanced by the heat conduction into the substrate. The heat conduction is determined by the temperature gradients in the solid. For the case of pulsed-laser annealing, the temperature gradients are initially established by the energy-absorption profile of the incident laser energy in the substrate. Included in the numerical calculations were temperature-dependent values of the thermal conductivity, heat capacity, and electrical conductivity. Specific values of the parameters used in the calculations are listed in Table I. Free-carrier-absorption[24] effects in solid Si have been included in the numerical calculations by adjusting the optical-absorption length to reproduce the measured melt-threshold energy density.

Figure 5 shows both experimental melt-depth—versus—time data and the melt depths calculated numerically. As is evident from the figure, the agreement between calculations and experiment is excellent. Consequently, the thermal model for melting and resolidification during pulsed-laser annealing completely describes the behavior observed experimentally in the time regimes we have studied.

C. Solidification velocity

The solidification-front velocity v is determined by the rate at which heat released at the advancing liquid-solid interface $v\Delta H$ is conducted into the substrate by thermal diffusion $\kappa\,\partial T/\partial z$, as shown by

$$v=\frac{\kappa}{\Delta H}\frac{\partial T}{\partial z}\ , \tag{5}$$

where κ is the thermal conductivity, ΔH is the latent heat of fusion, and $\partial T/\partial z$ is the thermal gradient normal to the solidification front. This model assumes the liquid-solid interface to be planar and stable. The good agreement between the experimental results and the calculations (Fig. 5) justifies these assumptions. Figure 6 shows the solidification-front velocity as a function of time for various incident laser energy densities. The velocity is obtained by numerically differentiating the melt-depth—

TABLE I. Parameters used in numerical calculations, where T is the temperature in K.

Parameter	Value
κ, thermal conductivity[a]	$1585T^{-1.23}$ W/cm K, $T<1370$ K
	0.221 W/cm K, $T\geq 1370$ K
ρ, electrical resistivity[b]	$2528\exp[0.00479\ (1685-T)]$ $\mu\Omega$ cm (solid)
	80 $\mu\Omega$ cm (liquid)
C_p, heat capacity[c]	$(1.978+3.54\times10^{-4}T)-(3.68\times10^{4}T^{-2})$ J/cm^3 K
ΔH, enthalpy of fusion[c]	4206 J/cm^3
T_m, melting temperature[c]	1685 K
R, optical reflectivity	38% (solid), 71.8% (liquid)
α, optical-absorption length	0.91 μm (solid), 0.025 μm (liquid)

[a]Reference 25.
[b]Reference 26.
[c]Reference 27.

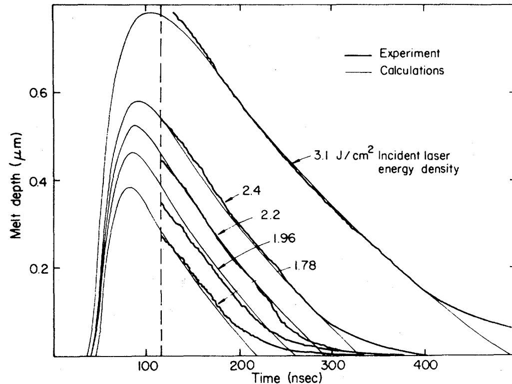

FIG. 5. Experimental (heavy solid line) and computer-calculated (light solid line) melt depths as a function of time for several incident laser energy densities above the melt threshold. Dashed line indicates the duration of the photoresponse which obscures the melt-depth information in the experimental data.

versus–time data of Fig. 5. Equation (5) shows that the velocity is determined by the thermal gradient. In the case of pulsed-laser irradiation, the initial thermal gradient is established by the absorption profile of the laser irradiation in the solid. Consequently, for short times near the end of the laser pulse, thermal diffusion does not influence the thermal gradients. At times which are long compared to the irradiation time ($t > 150$ nsec in the work presented here), thermal diffusion determines the thermal gradients.

Detailed calculations of the regrowth dynamics require numerical methods to solve the nonlinear differential equations involved as presented in Sec.

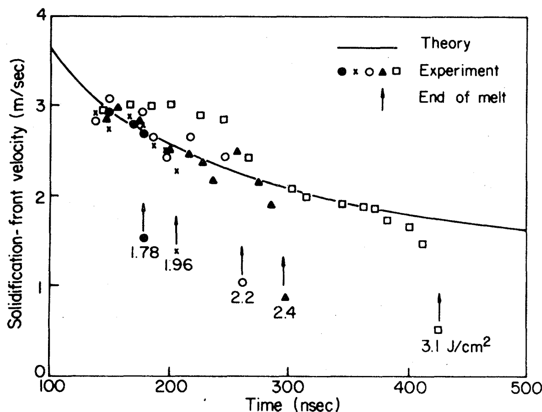

FIG. 6. Experimental (symbols) solidification-front velocity as a function of time obtained by numerical differentiation of the data in Fig. 5. Solid line shows the $v \propto t^{-1/2}$ calculated velocities from Eq. (7). Arrows indicate the time at which resolidification is complete.

IV B. These calculations were shown to be in excellent agreement with experimental results (Fig. 5). It is also possible to make approximations which lead to very simple equations for the resolidification velocity in the thermal-diffusion regime (i.e., at long times). These equations again show the applicability of the thermal model and allow the experimenter a first-order check on the data without resorting to numerical calculations. An expression for the solidification-front velocity in the thermal-diffusion-limited regime can be obtained by neglecting the temperature dependence of the thermal conductivity and by making a linear approximation to the temperature profile in the solid using a gradient

$$\frac{\partial T}{\partial z}=\frac{T_m-298}{2\sqrt{Dt}} \tag{6}$$

determined by the thermal-diffusion length, where D is the thermal diffusivity ($D=\kappa/C_p \simeq 0.1$ cm^2/sec using values for κ and C_p from Table I at temperatures near T_m) and t is time. The thermal gradient [Eq. (6)] is used in Eq. (5) to obtain the following expression for the solidification-front velocity, in units of m/sec,

$$v=\frac{\kappa}{\Delta H}\frac{T_m-298}{2\sqrt{Dt}}=\frac{1.15\times 10^{-3}}{\sqrt{t}} . \tag{7}$$

The velocity obtained from Eq. (7) is plotted in Fig. 6 for comparison with the experimental results. Numerical differentiation of the melt-depth data to obtain velocity data enhances differences between experiment and theory. Nevertheless, the predictions of Eq. (7) agree well with both experiment, Fig. 6, and with the detailed numerical calculations.

Although the solidification-front velocity is not constant in time [Eq. (7)], it is desirable for the purposes of discussion and comparison to have a single value for the velocity. An approximate velocity such as this can be obtained by making a straight-line fit to the melt-depth–versus–time data. Figure 7 shows the approximate solidification-front velocities $\bar{v}$ obtained using straight-line fits to the data in Fig. 5.

Equation (3) shows that the photoconductance and the conductance due to thermal carriers contribute linearly to the observed conductance. Consequently, the photoconductance, obtained from data at incident laser energy densities below the melt threshold, could be subtracted from the observed conductance. However, in practice the numerical inaccuracies introduced by subtracting two digitized curves are unacceptably large. Therefore, the experimental results presented in this paper are all for times (>115 nsec) by which the photoconductance has decayed to a negligibly small value. A simple calculation of the conductance due to thermal car-

riers σ_t in the hot substrate behind the solidification front can be made using the approximate thermal gradient from Eq. (6). Equation (6) is used to obtain an approximate equation for the temperature as a function of distance z into the substrate,

$$T(z)=T_m-\frac{\partial T}{\partial z}z \ . \tag{8}$$

The largest conductance by thermal carriers will occur immediately upon termination of the melt. Consequently, the following calculations will be for $t'=400$ nsec as an example of the largest effect σ_t can have on the melt depth. The expression for electrical resistivity from Table I, using Eq. (8) for the temperature, is integrated over the thermal-diffusion length to obtain the total thermal-carrier contribution to the conductance in units of Ω^{-1} at time t',

$$\sigma_t(t')=\int_0^L\frac{dz}{\rho}=A\int_0^L e^{-Bz}dz$$
$$=\frac{A}{B}(e^{-BL}-1)=0.024 \ , \tag{9}$$

where $L=2\sqrt{Dt'}=4\times10^{-4}$ cm, $A=395.6$ Ω^{-1}cm^{-1}, and $B=166\,09$ cm^{-1}. The effect of the thermal contribution can be considered by expressing the conductance [Eq. (9)] as an effective melt in units of μm at time t',

$$d_{\rm eff}=R\sigma_t\rho\frac{l}{w}=0.014 \ , \tag{10}$$

where R is the ratio of the conductance in the liquid phase to the conductance in the solid phase at T_m ($R=\frac{1}{31.6}$), ρ is resistivity of molten Si, and l/w is the length-to-width ratio of the sample. Equation (10) shows the conductance due to thermal carriers has a small affect on the melt-depth results.

D. Melt duration and threshold energy

For short melt durations, i.e., at low energies, there is insufficient time for thermal diffusion to substantially alter the thermal gradients established by the absorption of the laser energy. As it is the thermal gradients which determine the solidification-front velocity, the velocity is relatively independent of laser energy in this short-melt-duration regime. Figure 7 shows that the velocity is indeed constant (2.85 m/sec) for incident laser energy densities less than 2.3 J/cm^2. Since the maximum melt depth increases linearly with increasing laser energy above the melt threshold (Fig. 5), the melt duration should increase linearly with energy in the low-energy regime ($E<2.3$ J/cm^2) where the velocity is constant. Figure 8 shows the melt duration as obtained from optical-reflectance data as a function of incident laser energy density. At higher

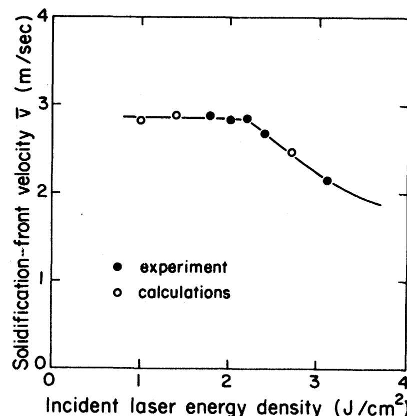

FIG. 7. Solidification-front velocity $\bar{v}$ as a function of incident laser energy density obtained from straight-line fits to the experimental melt-depth data in Fig. 5 (solid circles) and to the calculated melt-depth data (open circles).

energies, thermal diffusion reduces the thermal gradients and the velocity decreases with increasing laser energy density. Figure 7 shows that the solidification velocity is approximately inversely proportional to laser energy density for energy densities greater than 2.3 J/cm^2. Consequently, the melt duration (Fig. 8) should increase approximately as the square of the laser energy density for energy

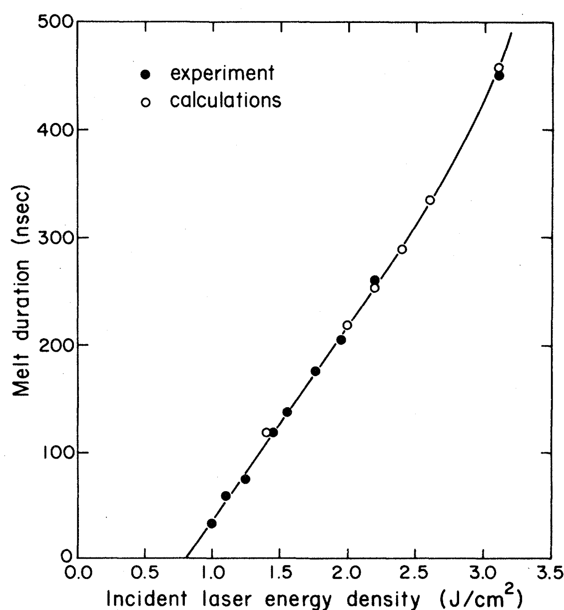

FIG. 8. Melt duration as a function of incident laser energy density obtained from optical-reflectance data (solid circles) and from computer calculations (open circles).

densities greater than 2.3 J/cm^2. Similar results have been reported by Auston and co-workers.[1]

The threshold energy density for melting can also be obtained from optical-reflectance measurements and is found to be $\sim$0.8 J/cm^2, in agreement with the energy-absorption data of Sec. III C.

V. CONCLUSIONS

Interaction of high-energy pulsed-laser irradiation and single-crystal Si results in an ultrarapid melt-quench process. The rate of this quenching, as characterized by the velocity of the resolidification front, is of considerable practical and theoretical importance. In this paper we have used *in situ* conductance measurements to measure this resolidification- (liquid-solid interface) front velocity and found the results to be in agreement with calculations based on a thermal model. The solidification-front velocity is controlled by the rate at which heat is removed from the liquid-solid interface by thermal conduction. Thermal conduction is in turn controlled by the thermal gradient normal to the interface. Consequently, control of the solidification-front velocity is obtained by control of the thermal gradient. In pulsed-laser irradiation, where the pulse duration is short compared to the time required for appreciable thermal diffusion, the thermal gradients are initially established by the absorption of the laser energy in the solid. Hence, the optical properties of the irradiated material, in addition to the thermal properties, play an important role in the annealing dynamics. Consequently, the solidification velocity can be affected by varying the laser-pulse length, wavelength, and energy. The velocity can be further affected by varing the thermal properties of the sample material and by varying the ambient temperature of the sample.

Control of the solidification-front velocity allows experimental observation of the effects of the velocity on segregation and trapping of impurities. Furthermore, studies can be made of the dynamic behavior of the liquid-solid interface. At sufficiently high velocities, silicon is found to resolidify in the amorphous state since the interface moves more rapidly than the atoms can move to crystalline sites.[28]

The transient techniques, electrical conductance and optical reflectance, allow experimental measurement of the melting and resolidification dynamics. Time-resolved measurement of the electrical conductance allows direct calculation of the solidification-front velocity. If the carrier lifetime is sufficiently short, as in silicon on sapphire, this measurement can also provide the melt-front velocity. Simultaneous measurement of the conductance and the reflectance provides both complementary information (e.g., melt depth from conductance and melt start time from reflectance) and corroboration (e.g., melt duration from both techniques).

The absorbed-energy measurements provide necessary data on the energy coupling between the laser and the sample. Not only is this information necessary for accurate numerical simulations of laser melting and solidification dynamics, it also enables many interesting experiments on the physics of the energy coupling.

This paper has presented the application of these measurements to Au-doped single-crystal silicon. The electrical-conductance technique uniquely provided measurement of the melt depth and solidification-front velocity. For the experimental regime studied, i.e., 30-nsec ruby laser operating over the range of (0.8—3.1)-J/cm^2 incident energy densities, melt durations were found to be up to 450 nsec and solidification velocities were observed over the range of 2—3 m/sec. All of these results were found to be in excellent agreement with a thermal melting model.

ACKNOWLEDGMENTS

The authors would like to thank E. L. Neau of Sandia National Laboratories for use of the transient digital analyzer. One of us (M.T.) would like to acknowledge support from a National Science Foundation graduate fellowship. This work was in part supported by the U. S. Defense Advanced Research Projects Agency through the U.S. Office of Naval Research and by the U.S. Department of Energy under Contract No. DE-AC04-76-DP00789.

---

[1]D. H. Auston, J. A. Golovchenko, A. L. Simons, R. E. Slusher, P. R. Smith, C. M. Surko, and T. N. C. Venkatesan, in *Laser-Solid Interactions and Laser Processing—1978*, edited by S. D. Ferris, H. J. Leamy, and J. M. Poate (AIP, New York, 1979), p. 11.

[2]C. W. White, J. Narayan, and R. T. Young, Science 204, 461 (1979).

[3]J. Narayan and C. W. White, in *Laser and Electron Beam Processing of Materials,* edited by C. W. White and P. S. Peercy (Academic, New York, 1980), p. 65.

[4]W. L. Brown, in *Laser and Electron-Beam Solid Interactions and Materials Processing,* edited by J. F. Gibbons, L. D. Hess, and T. W. Sigmon (North-Holland, New York, 1981), p. 1.

[5]J. Narayan, J. Fletcher, C. W. White, and W. H. Christie, J. Appl. Phys. 52, 7121 (1981).

[6]N. Bloembergen, in *Laser-Solid Interactions and Laser Processing—1978,* edited by S. D. Ferris, H. J. Leamy, and J. M. Poate (AIP, New York, 1979), p. 1.

[7]J. C. Wang, R. F. Wood, and P. P. Pronko, Appl. Phys. Lett. 33, 455 (1978).

[8]J. A. Van Vechten, R. Tsu, and F. W. Saris, Phys. Lett. 74A, 422 (1979).

[9]H. W. Lo and A. Compaan, Phys. Rev. Lett. 44, 1604 (1980).

[10]P. Baeri, J. M. Poate, S. U. Campisano, G. Foti, E. Rimini, and A. G. Cullis, Appl. Phys. Lett. 37, 912 (1980).

[11]J. Narayan, J. Appl. Phys. 52, 1289 (1981).

[12]A. G. Cullis, H. C. Webber, D. V. McCaughan, and N. G. Chew, in *Laser and Electron Beam Processing of Materials,* edited by C. W. White and P. S. Peercy (Academic, New York, 1980), p. 183.

[13]G. J. Galvin, M. O. Thompson, J. W. Mayer, R. B. Hammond, N. Paulter, and P. S. Peercy, Phys. Rev. Lett. 48, 33 (1982).

[14]M. O. Thompson, G. J. Galvin, J. W. Mayer, R. B. Hammond, N. Paulter, and P. S. Peercy, in *Laser and Electron Beam Interactions with Solids,* edited by B. R. Appleton and G. K. Celler (North-Holland, New York, 1982), p. 209.

[15]Michael O. Thompson, G. J. Galvin, J. W. Mayer, P. S. Peercy, and R. B. Hammond, Appl. Phys. Lett. (in press).

[16]P. S. Peercy and W. R. Wampler, Appl. Phys. Lett. 40, 768 (1982).

[17]S. M. Sze, *Physics of Semiconductor Devices* (Wiley, New York, 1969), p. 49.

[18]A. G. Cullis, H. C. Webber, and P. Bailey, J. Phys. E 12, 688 (1979).

[19]R. F. Wood and G. E. Giles, Appl. Phys. Lett. 38, 422 (1981).

[20]A. V. Dvurechensky, G. A. Kachurin, T. N. Mustafin, L. S. Smirnov, in *Laser-Solid Interactions and Laser Processing—1978,* edited by S. D. Ferris, H. J. Leamy, and J. M. Poate (AIP, New York, 1979), p. 245.

[21]T. E. Faber, *Introduction to the Theory of Liquid Metals* (Cambridge University Press, Cambridge, England, 1972), p. 326.

[22]P. Baeri, S. U. Campisano, G. Foti, and E. Rimini, J. Appl. Phys. 50, 788 (1979).

[23]R. F. Wood and G. E. Giles, Phys. Rev. B 23, 2923 (1981).

[24]A. Lietoila and J. F. Gibbons, Appl. Phys. Lett. 34, 332 (1979).

[25]C. Y. Ho, R. W. Powell, and P. E. Liley, J. Phys. Chem. Ref. Data 1, 394 (1972).

[26]V. M. Glazov, S. N. Chizhevskaya, and N. N. Glagoleva, *Liquid Semiconductors* (Plenum, New York, 1969), p. 60.

[27]*CRC Handbook of Chemistry and Physics* (Chemical Rubber Company, Boca Raton, 1980).

[28]A. G. Cullis, H. C. Webber, and N. G. Chew, in *Laser and Electron Beam Interactions with Solids,* edited by B. R. Appleton and G. K. Celler (North-Holland, New York, 1982), p. 131.